

# Removal of Poly- and Perfluoroalkyl Substances from Natural and Wastewater by Tailored Silica-Based Adsorbents

Oksana Dudarko,\* Tetyana Budnyak, Oleg Tkachenko, Tatiana Agback, Peter Agback, Björn Bonnet, Lutz Ahrens, Geoffrey Daniel, and Gulaim Seisenbaeva\*



Cite This: *ACS EST Water* 2024, 4, 1303–1314



Read Online

ACCESS |

 Metrics & More

 Article Recommendations

 Supporting Information

**ABSTRACT:** Per- and polyfluoroalkyl substances (PFAS) are very stable and ubiquitously distributed in terrestrial and aquatic environments, and treatment and remediation techniques for the removal of PFAS are urgently needed. In this study, mesoporous silica matrix SBA-15 grafted with alkyl amino groups was used to remove perfluorooctanoate (PFOA) from aqueous solutions. The amino groups were grafted onto SBA-15 by the condensation of alkyl amino silanes. The synthesized adsorbents were studied by SEM, TEM, IR, low-temperature nitrogen sorption, and XRD. The solid-state and liquid  $^{19}\text{F}$  NMR spectroscopy, EDX, and LC-MS/MS results showed high adsorption efficiency and rapid reaction kinetics. In freshly prepared solutions and on the surface of the sorbents, the presence of PFOA micelles was observed. Furthermore, the introduction of amine-containing groups into the structure of the sorbent allows the sorption of up to 649 mg/g of PFOA from solutions. Results showed that the protonated surface amino groups and PFOA interacted electrostatically. The obtained results open perspectives for producing adsorbents for facile extraction of PFAS.

**KEYWORDS:** PFAS, PFOA, sorption, SBA-15, water treatment



## INTRODUCTION

Continued use of fossil fuels around the world is associated with the risks of large-scale fires. The result of this is increasing use of fire extinguishing agents class B, especially when oil containers, cars, etc., are involved. The same can be said of areas that experience military conflicts, where in addition to the direct consequences, there occurs environmental disasters due to the massive use of fire extinguishing agents.<sup>1</sup>

Perfluorooctanoate (PFOA) has been detected in drinking water, seawater, groundwater, and other natural water sources because it has high resistance to degradation and high mobility in the aqueous environment.<sup>2</sup> A recent study found that perfluoroalkyl acids (PFAAs) such as PFOA are difficult to remove and can serve as a good model in studies of PFAS.<sup>3</sup> There is an urgent need to develop energy- and cost-efficient methods to remove or degrade PFOA into harmless species because of its potential toxicity to living organisms.<sup>4</sup> PFOA and perfluorooctanesulfonate (PFOS) practically do not degrade in nature, and due to their anionic nature, they also possess high water solubility.<sup>5</sup> The uniqueness of PFAS such as PFOA is due to both hydrophobic and lipophobic characteristics, which causes a wide application of PFAS in products and industries.<sup>6</sup>

A new EU Drinking Water Directive (2020/2184) for PFAS has been decided by the European Parliament and Council including a limit of 100 ng/L for  $\sum_{20}\text{PFAS}$  and a limit of 500 ng/L for the sum of organofluorine.<sup>7</sup> Thus, new drinking water guidelines need to be implemented in national regulations

within the EU, which fulfill at least the standard of the EU Drinking Water Directive. For example, the Swedish Food Agency has adopted new drinking water regulations with 100 ng/L for  $\sum_{21}\text{PFAS}$ , 500 ng/L for the sum of organofluorine, and 4 ng/L for  $\sum_{4}\text{PFAS}$  (LIVSFS 2022:12). The limit value for  $\sum_{4}\text{PFAS}$  includes PFOA, perfluorononanoate (PFNA), perfluorhexanesulfonate (PFHxS), and PFOS, which are based on the EFSA health-based guidelines.<sup>8</sup> The limit value for  $\sum_{21}\text{PFAS}$  covers the  $\sum_{20}\text{PFAS}$  substances specified in the EU Drinking Water Directive plus 6:2 fluorotelomer sulfonate (FTSA).<sup>9</sup>

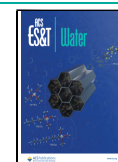
The removal of PFAS from water by using traditional treatment technologies, such as biological degradation, oxidation, and reduction, has been ineffective because of the unique physicochemical properties of these compounds (e.g., extremely high persistence).<sup>10–12</sup> Decomposition of PFOA requires high temperatures or specific chemicals, which makes the process costly.<sup>13</sup> Alternative treatments (oxidative and photocatalytic processes, sorption by anion exchange and activated carbon, and membrane technologies) have been

**Received:** July 24, 2023

**Revised:** December 27, 2023

**Accepted:** December 27, 2023

**Published:** January 13, 2024



developed to improve the removal efficiency of PFAS from soils and aquatic environments.<sup>14,15</sup> Membrane technologies are generally the most effective in removing these compounds but are expensive to operate and retain a relatively high concentrated PFAS solution (retentate) and a relatively high volume compared with other separation technologies. The obtained retentate has often required further processing before its disposal.<sup>16,17</sup> In contrast, adsorption processes have shown high removal efficiency for PFAS and can be more cost-effective.<sup>18–20</sup> Another advantage of adsorption techniques is the easy implementation of existing treatment systems and stability of operation.<sup>21–23</sup> However, it is important to improve our understanding of the sorption characteristics, such as adsorptive affinity and surface capacity, for PFAS removal.

This study aimed to develop highly efficient and regenerable tailored silica-based sorbents for the removal of PFOA as a representative of perfluoroalkylated acids (PFAA) and to reveal the sorption mechanisms of PFOA to the sorbents. Amine-containing materials derived from ordered mesoporous silica developed by the University of California at Santa Barbara, SBA-15 (SBA-NH, SBA-DA, SBA-TA—for detailed description, please, see later) were selected as the sorbent for PFAS removal as it has demonstrated high capacity and selectivity in relation to various types of pollutants.<sup>24–28</sup> Different ligands were used because the basic properties of the amino group usually are enhanced by the influence of alkyl radicals so primary amines are stronger bases than ammonia, which could be explained by the electron-donating properties of alkyl radicals (induction effect). The electron-donating methyl group makes the secondary amino groups (SAGs) stronger bases than the primary amino group (PAG). Therefore, in this work, the following amino ankoxyisilane has been used: APTES (3-aminopropyl)triethoxysilane contains only PAG, TPEDA (*N*-[3-(trimethoxysilyl)propyl]ethylenediamine) contains both PAG and SAG, and TPETA N1-(3-trimethoxysilylpropyl)-diethylenetriamine contains three amino groups of PAG and two amino groups of SAG.

Hereby, the role of the alkyl chain length of the amino cation and the density of its grafting on the surface were investigated in order to assess the sorption capacity for PFOA as well as the pollutant uptake mechanisms.

## MATERIALS AND METHODS

**Chemicals.** All chemicals used in this study, including sodium metasilicate (SS, NaSiO<sub>3</sub>·5H<sub>2</sub>O), APTES (H<sub>2</sub>N-(CH<sub>2</sub>)<sub>3</sub>Si(OC<sub>2</sub>H<sub>5</sub>)<sub>3</sub>), Pluronic 123 (P123), TPETA ((CH<sub>3</sub>O)<sub>3</sub>Si(CH<sub>2</sub>)<sub>3</sub>NHCH<sub>2</sub>CH<sub>2</sub>NHCH<sub>2</sub>CH<sub>2</sub>NH<sub>2</sub>, techn. grade), TPEDA ((CH<sub>3</sub>O)<sub>3</sub>Si(CH<sub>2</sub>)<sub>3</sub>NHCH<sub>2</sub>CH<sub>2</sub>NH<sub>2</sub>, 97%), hydrochloric acid (HCl) (37%, w/w), and ethanol, were purchased from Merck (Darmstadt, Germany) and Sigma-Aldrich (St. Louise, Missouri, USA). PFOA (with a purity of >90%) was obtained from Fluka Chemical (Switzerland).

**Adsorbent Matrix Preparation. Synthesis of SBA.** The pure SBA-15 (sample SBA) was prepared according to previous publications with some modifications.<sup>29,30</sup> Briefly, 2.5 g of surfactant (Pluronic 123) was dissolved in 70 mL of 2 M HCl during constant stirring for 30 min at room temperature giving a transparent solution. 0.05 mol of SS, separately dissolved in 20 mL of water, was added in a thin stream to the resulting clear mixture. Sedimentation began immediately and ended after about 2 min. The resulting heterogeneous system was further stirred for 2 h at 40 °C. After that, hydrothermal treatment (HTT) was performed at

80 °C for 20 h, followed by the filtration of the white precipitate. The resulting precipitate was dried in air overnight, and the template was removed by boiling in acidified ethanol four times with stirring for 3 h. The filtered material was dried in vacuum for half an hour at room temperature and then another half an hour at 50 °C and another 3 h at 100 °C.

**Synthesis of SBA-NH/SBA-DA/SBA-TA.** 2.44 g of surfactant (Pluronic 123) was dissolved in a mixture of 24.4 mL of H<sub>2</sub>O and 22.4 mL of HCl<sub>conc</sub> on constant stirring for 30 min at room temperature giving a transparent solution. Then, 0.008 mol of APTES (SBA-NH), TPEDA (SBA-DA), and TPETA (SBA-TA) was added and the template solution stirred for 5 min. 0.04 mol of SS, separately dissolved in 32 mL of water, was added in a thin stream to the resulting clear mixture. Sedimentation began immediately and ended after about 5 min. All further treatment procedures were the same as those for SBA synthesis.

**Characterization.** Scanning electron microscopy (SEM) studies were carried out with a Hitachi FlexSEM 1000II instrument equipped with energy-dispersive X-ray spectrometry (EDX) (Oxford Instruments). For transmission electron microscopy (TEM), dispersions of adsorbent particles were deposited on holey carbon grids (Pelco 50 mesh grids: Pitch 508 μm; hole width 425 μm; bar width 83 μm; transmission 70%) and observed using a Philips CM/12 microscope (Thermo Fisher Inc.) fitted with a LaB6 gun and operated at 100 kV. Fourier transform infrared (FTIR) analysis was performed with a PerkinElmer Spectrum 100 FTIR spectrometer using KBr pellets. Thermogravimetric (TG) analyses were carried out using a PerkinElmer Pyris 1 thermobalance with control of outgoing gases using a PerkinElmer Spectrum 100 instrument that was also used separately for vibration spectrometry measurements. Determination of the total groups' content was carried out by CHNS combustion analysis. Small-angle X-ray scattering (SAXS) patterns were obtained using a DRON-4-07 diffractometer (CuKα) radiation (λ = 1.5418 Å) in the small-angle range (2θ = 0.5–5.0). The values of the specific surface area and pore volume/size were determined from nitrogen adsorption/desorption isotherms at –196 °C (Micromeritics ASAP 2020 Surface Area and Porosity Analyzer, Norcross, GA, USA). Samples were degassed at 120 °C for 3 h in a vacuum before the measurements. Concentrations of available functional groups on the mesoporous silica surfaces were determined by conductometric titrations with aqueous solutions of HCl and NaOH using a Metrohm Titrand 888 (2.888.0310), fitted with an 856 conductivity module (2.856.0010), 800 Dosino (2.800.0010), and five-ring conductivity measuring cell (c = 0.7, 6.0915.100), using TIAMO Light 2.5 as automation software. Titrers were determined using tris(hydroxymethyl)-aminomethane (HCl) and potassium hydrogen phthalate (NaOH). Amine content was determined via conductometric titration by direct and back-titration of the protonated amine. Titration was also carried out in the absence of silica to determine the dependence of the electric conductivity (k) on the acid concentration.

The sorption properties of the synthesized composites were studied under static conditions, initially on the model solutions of PFOA. Kinetics and thermodynamics of adsorption processes were studied following PFOA uptake versus time and versus solution concentrations respectively (adsorption isotherms).

Liquid-state  $^{19}\text{F}$  NMR experiments were conducted on 600 MHz Bruker Avance III spectrometers equipped with a smart probe at a temperature of 298 K. For intensities calibration of the resonances in the 1D  $^{19}\text{F}$  spectrum, a synthetic eretic signal was used and placed in every spectrum at 90 ppm as an external standard. Its intensity was calibrated to a concentration of 0.3 mM. Spectra were processed by TopSpin4.2.0. Solid-state  $^{19}\text{F}$  NMR measurements were performed on a 600 MHz Bruker Avance III spectrometer using a 4 mm H-F/BB CP-MAS probe. The samples were packed into 4 mm  $\text{ZrO}_2$  rotors. Spectra were recorded at 10 kHz at room temperature using the one pulse experiment with a relaxation delay of 5 s. Sweep width was 354 ppm, and 16 scans were collected.

The sorption properties of the synthesized composites were studied under static conditions, first on the model solutions of PFOA. The initial solution with a concentration of 0.1 mol/L was prepared from a portion of PFOA in methanol. Then, it was diluted to the required concentration with water. Sample weights of 0.02 g were filled with 5 mL of PFOA solutions from 0.001 to 0.016 mol/L in order to study the effect of the concentration on the sorption capacity. The study of kinetics was carried out by measuring the concentration of PFOA after 0.25, 0.5, 1, 6, and 12 h. The initial concentration was 0.00008 mol/L. The pH measurement showed that the pH of the aqueous solutions of the samples is approximately 3.0, and the pH of the solutions after PFOA sorption is 2.2 for all points. The choice of pH was based on literature data, where pH = 3 was optimal. Kinetics and thermodynamics of adsorption processes were investigated following the PFOA uptake versus time and versus solution concentrations, respectively (adsorption isotherms). Analysis of target PFOA was performed by liquid chromatography coupled to tandem mass spectrometry (LC-MS/MS) on a Sciex Triple Quad 3500 system with a Phenomenex Gemini 3  $\mu\text{m}$  C18 HPLC column as an analytical column, a Phenomenex KJ0-4282 guard column, and a Phenomenex Kinetex 1.7  $\mu\text{m}$  C18 delay column. A nine-point calibration curve (0.01–100 ng  $\text{mL}^{-1}$ ) in 50/50% Milli-Q/methanol was used for quantification (for more details, see Smith et al.<sup>31</sup>). Data evaluation was performed in SciexOS (Sciex, USA). After adsorption, the solution was drained by decantation, then centrifuged for 5 min at a speed of 3000 and taken with a syringe with a filter so that the sample particles did not get into it. After sorption, 50  $\mu\text{L}$  of the solution was diluted with water to 50 mL, and 5 samples were taken from it for analysis. Samples were prepared by direct injection. In short, 0.5 mL of PFOA aqueous solution was mixed with 0.4 mL methanol and 0.1 mL internal standard (Wellington Laboratories, MPFAC-24ES mixture) containing  $^{13}\text{C}_8$ -PFOA solution in methanol.

Two kinetics models, pseudo-first kinetic model (eq 1) and pseudo-second kinetic model (eq 2), were applied for approximation of kinetics data:

$$A_t = A_{\text{eq}} \times (1 - e^{-k_1 t}) \quad (1)$$

$$A_t = \frac{k_2 \cdot A_{\text{eq}}^2 \cdot t}{1 + k_2 \cdot A_{\text{eq}} \cdot t} \quad (2)$$

where  $A_{\text{eq}}$  and  $A_t$  are the adsorption, mg/g, in a state of equilibrium and at time  $t$ , min;  $k_1$  and  $k_2$  are the rate constants.

The initial rate of the sorption was estimated using the equation proposed by Ho:<sup>32</sup>

$$h_0 = k_n \times A_{\text{eq}}^n \quad (3)$$

where  $n$  is the order of the most suitable kinetic model.

The equilibrium isotherms were fitted by using the Langmuir model (eq 1) and Freundlich model (eq 2):

$$A_{\text{eq}} = \frac{A_{\text{max}} \times K_L \times C_e}{1 + K_L \times C_e} \quad (4)$$

$$A_{\text{eq}} = K_F \times C_e^{1/n_F} \quad (5)$$

where  $C_{\text{eq}}$  is the equilibrium concentration of the adsorbate in the solution, mg/L;  $A_{\text{max}}$  is the maximum adsorption capacity for complete one-layer surface coverage, mg/g;  $K_L$  and  $K_F$  are the Langmuir and Freundlich adsorption equilibrium constants; and  $n_F$  is an empirical parameter related to the intensity of adsorption and the heterogeneity of the adsorbent.

The fitting results were evaluated using the following statistical parameters: the adjusted determination coefficient ( $R_{\text{adj}}^2$ ) (eq 5) and the standard deviation (SD) of residues (eq 6), calculated according to equations:

$$R_{\text{adj}}^2 = 1 - (1 - R^2) \times \left( \frac{r - 1}{r - p - 1} \right) \quad (6)$$

$$\text{SD} = \sqrt{\frac{1}{r - p} \times \sum_i^r (A_{i,\text{model}} - A_{i,\text{exp}})^2} \quad (7)$$

where  $r$  and  $p$  are the total number of experimental points and fitting parameters, respectively; and  $A_{i,\text{model}}$  and  $A_{i,\text{exp}}$  are calculated and measured adsorptions of PFOA, respectively.

## RESULTS AND DISCUSSION

The micromorphology of the SBA-15-type silica particles was revealed by SEM with EDX showing aggregated pellet-like particles and elemental composition (Figures 1 and S1), and ordered mesoporous structure of the samples was demonstrated by TEM (Figure 2).

The small particle size and ordered mesoporous structure of SBA-15 are known to provide rapid adsorption and mass exchange.<sup>27,28,33</sup> Previously, SBA-15 was primarily obtained

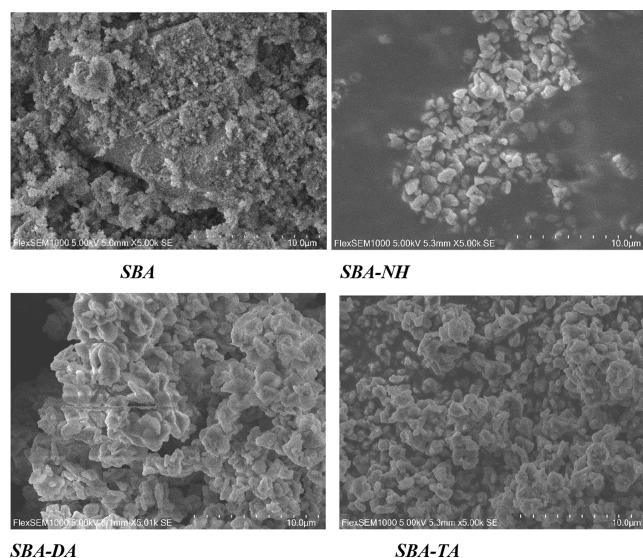
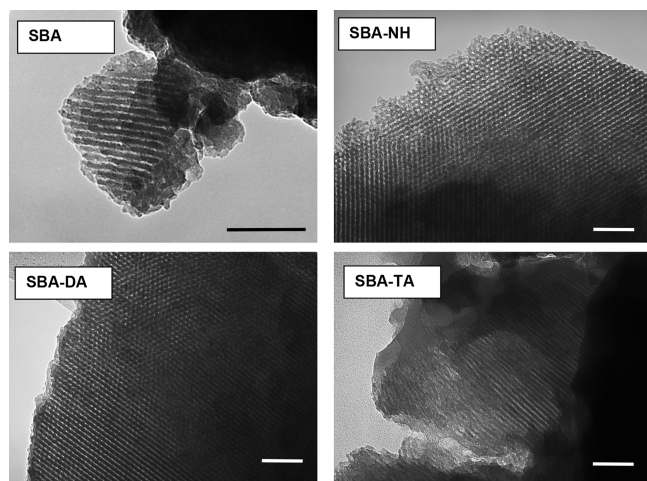


Figure 1. SEM images of the synthesized adsorbents.



**Figure 2.** TEM images of the synthesized samples. Bar lines = 100 nm.

using expensive tetraethyl ortho silicate as the silica precursor; therefore, an inexpensive sodium silicate as a source of silica has become an attractive option.<sup>29,30,34</sup> Using another source of silica than in our previous studies (i.e., solution of sodium silicate instead of solid salt) led to further characteristics of the samples especially of “bare” SBA-15. It provided particles of the nanosize that agglomerated into larger formations. In contrast, functionalized samples had approximately a uniform size and irregular shape of the primary particles. It was obvious that the presence of amino groups in the composition of trifunctional alkoxy silane affected the pH of the reaction mixture and resulted in the formation of larger particles.

The TEM data (Figure 2) showed that all the obtained samples had ordered centered rectangular hexagonal structures, as we expected. Channel-like structures running parallel to the longer direction, similar to the structure of SBA-15, were observed. The nature of the silica source and the ratio of

reagents in the reaction mixture, as well as the size of the functionalizing groups, influenced the process of structure formation. The particle pore sizes of all synthesized samples were measured along the (110) directions in the TEM images, showing 3–5 nm pores (Figure 2).

The thickness of the pore walls in all samples was in the range of 3–10 nm, also assuring their mechanical stability under sorption conditions.

X-ray patterns of functionalized samples contained a single sharp reflection at  $2\theta = \sim 0.91\text{--}0.98^\circ$  (Figure 3), corresponding to requirements of the 2D hexagonally ordered structures (symmetry group  $P6m$ ), and can be indexed as 100 (main XRD peak). At the same time, due to the presence of an amorphous phase in the samples, the two signals at 110 and 200 nm (two secondary reflection peaks) were not apparent (Figure 3). The XRD peaks of the samples are quite sharp, but their intensity is low, confirming the ordered structure observed by TEM (Figure 2).

Amino functional groups were introduced to induce specific sorption properties. The presence of a spatial network of siloxane bonds and functional groups in the samples was confirmed by IR spectroscopy (Figure 4). Functional amino

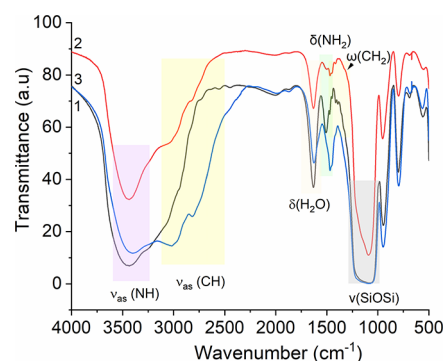


**Figure 4.** FTIR spectra of (1) SBA-NH, (2) SBA-DA, and (3) SBA-TA.

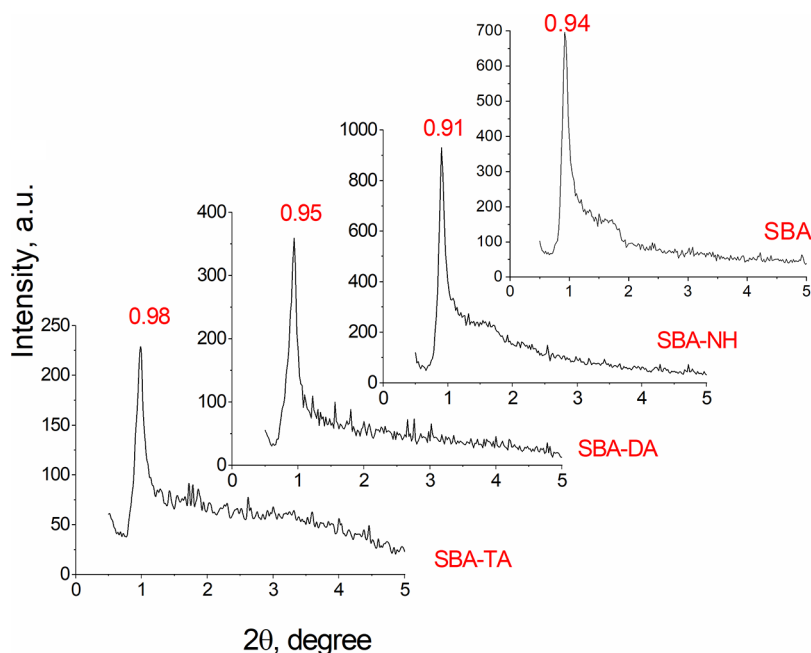


**Figure 3.** SAXS patterns for SBA, SBA-NH, SBA-DA, and SBA-TA.

**Table 1. Amount of Functional Groups for N-Containing Adsorbents (by Elemental and Titrimetric Analyses)**

sample	elemental analysis					conductometry	
	N, %	C, %	H, %	C/H ratio	C/N ratio	$C_L^a$ , mmol·g <sup>-1</sup>	$C_L$ , mmol·g <sup>-1</sup>
SBA-NH	2.81	8.97	3.95	2.6	3.2	2.0	1.3
SBA-DA	3.43	9.04	3.48	2.7	2.7	1.25	1.2
SBA-TA	5.14	13.21	4.94	2.8	2.6	1.3	0.4

<sup>a</sup>Content of grafted ligand.

groups in NH-containing samples were revealed by one intensive absorption band at 3430 cm<sup>-1</sup>, reflecting  $\nu_{\text{N-H}}$  stretching, and with a low-intensive band at 1508 cm<sup>-1</sup> attributed to bending  $\delta(\text{N-H})$ .

The analysis of CHNS elements proved that the content of nitrogen (i.e., presence of amino groups) in the adsorbent samples increased with the increase in the number of nitrogen atoms in the initial trialkoxysilanes used for functionalization. The percentage of nitrogen was in the range of 2.8–5.1%, and the amount of functional groups for polysiloxane samples was 1.3–2.0 mmol/g (Table 1).

The number of groups available for sorption was determined by conductometric titration. Calculations showed slightly underestimated data because of the partial protonation of the amino groups on the surface as a result of the template synthesis.

DTG and TG data were used to calculate the content of the organic components in the structure of the adsorbents (Figure S2). The content of physically adsorbed water or solvent residues used to wash the template for all samples was approximately in the range of 5.5–6.5% (0–150°C), while the percentage of organic components increased proportionally to the number and mass of introduced aminoorganosilyl groups. For SBA-NH in the interval 150–400 °C, the percentage weight loss was 10.5%, 13.1% for SBA-DA, and 22.1% for SBA-TA.

Nitrogen adsorption–desorption was performed to estimate the specific surface area of the synthesized materials. The parameters of the porous structure depended on the nature of the trifunctional alkoxy silanes. The porosity increased proportionally to the size of the organic nitrogen-containing component and the specific surface area and pore volume, while the average diameter of the pores decreased with a decrease in the surface area value (Table 2).

Using milder conditions (2 M HCl and sodium silicate solution) compared with our previous studies,<sup>28,29,29,34</sup> we obtained SBA based on metasilicate, with an ordered structure,

**Table 2. Textural Parameters of Obtained Mesoporous Samples<sup>a</sup>**

sample	$S_{\text{BET}}^1$ , m <sup>2</sup> ·g <sup>-1</sup>	$V_{\text{total}}^2$ , cm <sup>3</sup> ·g <sup>-1</sup>	$d_1$ , nm	$d_2$ , nm	average particle size, nm	$d_3$ , nm	$h_w^4$ , nm	$s_{a_0}^5$ , nm
SBA	314	0.37	6.1	7.2	19			
SBA-NH	248	0.33	4.7	6.8	24	7.7	3.6	11.3
SBA-DA	137	0.17	6.0	6.4	44	5.9	4.9	10.7
SBA-TA	77	0.10	3.5	6.4	77	4.6	5.8	10.4

<sup>a</sup>Notes:  $d$  denotes the diameter pores calculated by method: (1) BJH; (2) modified DFT; (3) from XRD; (4) width of the walls; (5) distance between the centers of pores (3–5 calculated by Bragg equations<sup>34,35</sup>).

but a slightly lower specific surface area. This can be observed not only from the TEM images (Figure 2) but also from the isotherm in Figure 5. The obtained low-temperature nitrogen adsorption–desorption isotherms, which have an S-shape belong to the type IV according to the IUPAC classification.<sup>36</sup> At 0.45–0.8  $p/p_s$ , the isotherms had a hysteresis loop characteristic of SBA-15 (Figure 5). According to the approach proposed previously,<sup>37</sup> the curves of pore size distribution were constructed (Figure 5b,c). It can be seen that the synthesized sorbents also contained micropores, characteristic of materials of the SBA-15 type.

**PFAS Removal Mechanisms.** PFOA is a surfactant; therefore, significant foaming and emulsion formation occur at the interface between the solvent and PFOA-contaminated water. It was reported earlier that electrostatic and hydrophobic interaction and self-aggregation (formation of micelles or hemimyces) are the most likely mechanisms involved in the adsorption of PFAS by amine-containing adsorbents of different nature, as shown in Deng et al.<sup>38</sup> and Dua et al.<sup>39</sup> Because the conditions of template synthesis provide the formation of protonated amino groups on the surface of the particles, the electrostatic attraction between positively charged functional groups on the adsorbent surface and anionic functional groups of PFAS is the driving force of adsorption. In this case, the pH of the solution affects its efficiency of adsorption as it can recharge the surface of the adsorbent, affecting the conditions of the electrostatic interaction. For most of the materials considered, the adsorption decreased with increasing pH of the solution with improved results in the acidic pH range.

<sup>19</sup>F chemical shifts are one of the most sensitive and commonly used NMR parameters that were applied to detect intramolecular interaction, for measuring the critical micelle concentration (CMC) of a surfactant.<sup>40–42</sup> In this study, samples of PFOA solutions with initial concentrations from 0.4 to 4 mg/mL were analyzed first by using <sup>19</sup>F NMR (Figure 6). The <sup>19</sup>F chemical shift of the  $-\text{CF}_3$  end group was shifted downfield to ca.  $-90$  ppm caused by intermolecular interactions. The <sup>19</sup>F chemical shifts of the  $-\text{CF}_2$  end groups are located between  $-110$  and  $-135$  ppm (Figure 6a). Moreover, the appearance of additional low-intensity peaks is observed (Figure 6a), which were also early attributed to reaching the CMC.<sup>43</sup> NMR measurements were repeated 5 days later to distinguish between these two sets of <sup>19</sup>F signals (Figure 6b).

As an example, the PFOA <sup>19</sup>F spectra with the lowest and highest concentrations next day and after 5 days, and solutions of PFOA after sorption by SBA-DA next day and after 5 days are shown in Figures S3 and S4. It is evident that the intensities of the <sup>19</sup>F signals after adsorption were decreased. Quantitative analysis was performed on samples from day 5 where the dependence of the intensities of the resonances for each sample was measured versus the initial concentration and type of adsorption matrix (Figure S5). It was concluded that the

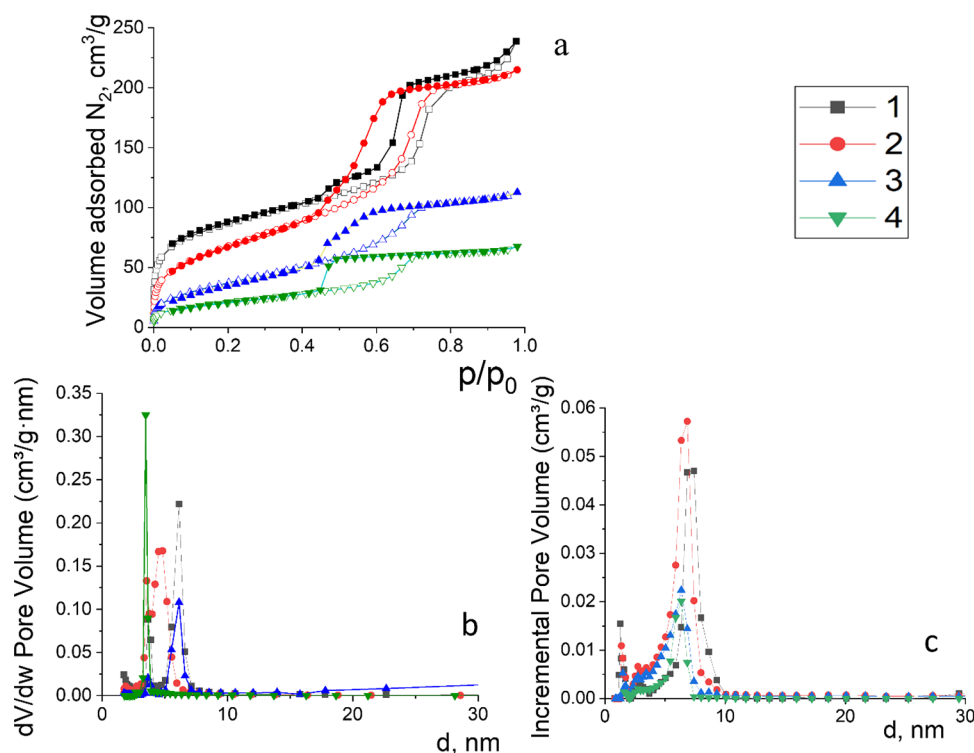


**Figure 5.** Low-temperature nitrogen adsorption–desorption isotherms (a), pore size distribution by BJH (b), and modified DFT (c). 1, SBA; 2, SBA-NH; 3, SBA-DA; and 4, SBA-TA.

most effective sorption was on samples: SBA-DA and SBA-TA, and the least adsorption was for bare SBA.

$^{19}F$  solid-state NMR spectroscopy permitted us to establish structural and quantitative information on the formed adsorption complexes based on the dispersion of the chemical shift of the  $^{19}F$  nuclei.  $^{19}F$  NMR was used to characterize unbound PFOA and its interaction with different surface types. In the spectra of the crystalline PFOA, only one peak associated with the  $CF_3$  end group (C-8) at  $-80.1$  ppm is detected (Figure 7(1)). Nevertheless, the spectra of adsorbed PFOA have different characteristics. There are two sets of signals of  $-CF_3$  at  $-79.6$  and  $-80.4$  ppm for SBA and SBA-DA (Figure 7(2,3)) and the high-field signals of  $-CF_3$  from  $-81.2$  to  $-82.0$  ppm for SBA-TA. Low-intensity peaks were attributed to a PFOA monomer with a higher diffusion rate, and higher intensity and peak broadening were attributed to PFOA micelles. It is evident that by increasing the concentration of  $-NH_3^+$  groups from SBA-DA to SBA-TA, the amount of monomers constituted with narrower line width is decreased, as long as the aggregated state is increased and observed online broadening resonances of  $^{19}F$  of PFOA.<sup>44</sup>

The  $^{19}F$  resonances at  $-115.4$  ppm observed for fluorine on  $C_2$  ( $\alpha$ , adjacent to the COOH group) and at  $-120.9$  ppm ( $\delta$ ,  $C_4$ ) (Figure 7(1,3,4)) are broadened compared to the corresponding resonances in the spectrum of PFOA on SBA-15 (Figure 7(2)). This is due to the interaction of both fluorine nuclei's with the surface amino-containing groups of the silica materials.

The spectrum of unbound PFOA (SBA) showed in the solid NMR spectrum well-resolved  $^{19}F$  signals, with slightly different chemical shifts than the corresponding resonances in the solution NMR spectra of the PFOA (Figure 6). This is in agreement with the NMR spectrum PFOA in.<sup>45</sup> It is noteworthy that the observed  $^{19}F$  resonances for PFOA

(SBA) have unusually, for solid NMR, narrow line width which can be attributed to the increased dynamics of PFOA in the matrix. That phenomenon can only take place if PFOA does not interact with the NH group. Additionally, in the spectrum of NH/PFOA complexes, due to the different environment of the  $^{19}F$  nuclei, the chemical shift is more dispersed compared to the unfunctionalized SBA (see Table 3).

The EDX data showed clearly an increase in the concentration of fluorine from pure SBA to functionalized samples (Figures 8, S6 and Table 4). Unfortunately, due to the low atomic weight, nitrogen was difficult to identify by EDX from the background of the other elements.

As shown in Figure 9, the absorbance at  $1775\text{ cm}^{-1}$  in the IR spectra corresponded to the C=O vibration of the carboxylic acid. It was still visible for 1 and 2 spectra, meaning that in SBA we observed physical sorption and COOH did not react with the surface. In the case of SBA-NH, the concentration of the NH group was lower than for SBA-DA and SBA-TA, and possibly some of the NH groups were not available for interaction with PFOA molecules, and the vibrations of COOH from PFOA and NH (at  $1503\text{ cm}^{-1}$ ) functional groups could be identified. Although there was a general similarity between the two spectra, spectra 3 and spectra 4 (Figure 9), significant changes in the carboxylate stretching region resulted from the presence of the sorbent. The  $\nu_s(\text{COO}^-)$  shifted to a slightly lower wavenumber (from  $1411$  to  $1408\text{ cm}^{-1}$ , marked by\*). All of the characteristic vibrational bands of C–F bonds were in the  $1300\text{--}1100\text{ cm}^{-1}$  range and superimposed with the vibrations of the Si–O–Si framework. Identifying the sorbed PFOA molecules interacting with NH groups was possible only by the disappearance of the bending vibration bands of the amino groups. After adsorption on silica, a shift of the vibrational band of water to  $1676\text{--}1689$

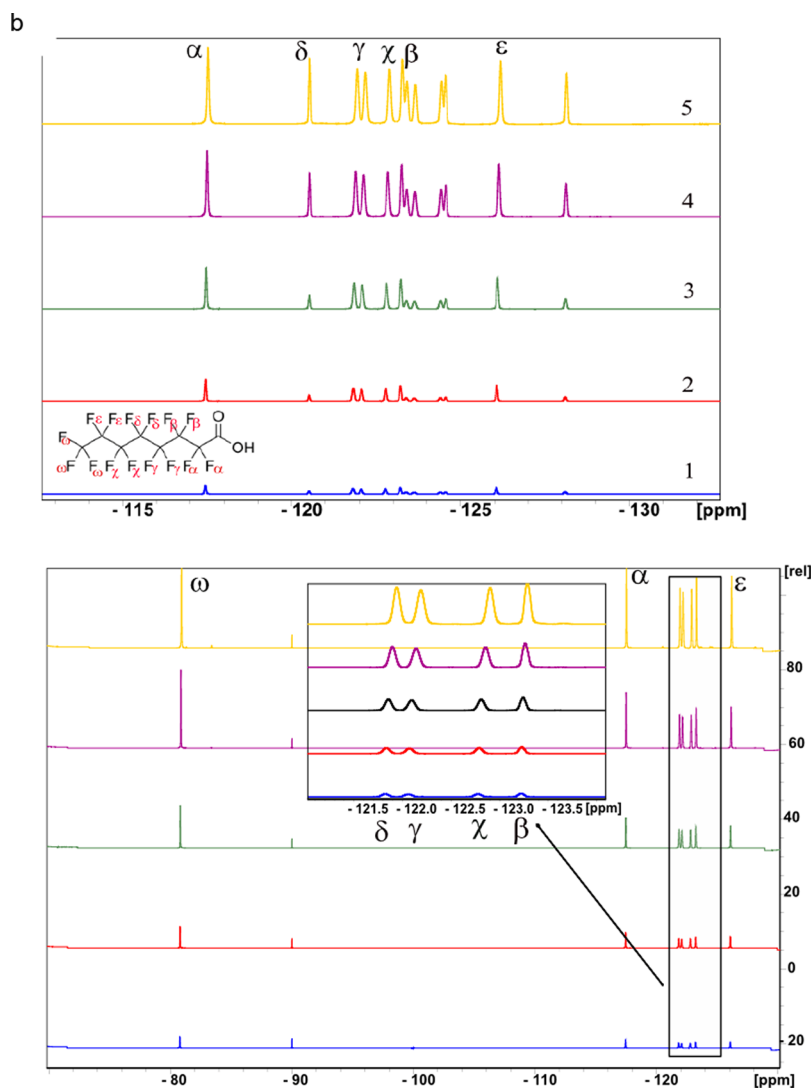


**Figure 6.** Solution state  $^{19}\text{F}$  NMR of the initial day one sorption of the solutions 0.001–0.012 mol/L ((a) 1 day after sample preparation and (b) 5 days later) for 1 = 0.001, 2 = 0.002, 3 = 0.004, 4 = 0.008, and 5 = 0.012 mol/L. In b region, (–120) to (–123) ppm is zoomed in and is presented in a separate window.

$\text{cm}^{-1}$  and the appearance of a band at  $1460\text{ cm}^{-1}$  (\*blue snowflake) corresponding to the asymmetric and symmetric stretching vibrations of the  $-\text{COO}$  groups, respectively, were observed.<sup>46</sup>

The effect of pH on the kinetics and capacity of PFOA adsorption has been studied repeatedly.<sup>47,48,49</sup> Lower pH results in faster adsorption and higher adsorption capacity. Under experimental conditions, PFOA predominantly existed in its corresponding deprotonated form ( $\text{p}K_{\text{a}} = 2.5$  for PFOA). The small diameter of the SBA particles meant that sorption occurred even due to the specific surface via electrostatic interaction of the hydroxyl groups of SBA and PFOA molecules. Features of the synthesis of SBA-15 functionalized with amino groups lead to the formation of protonated ammonium groups on the surface and on the walls of the pores of the particles.

As shown earlier, despite the low values of the specific surface of the synthesized materials, the structure was mostly ordered, and therefore, the availability of all functional groups for chemical interaction remained rather high. Therefore, the expected results were confirmed by the PFOA sorption

isotherms of our samples (Figure 10). For our experiments, we chose a pH close to that of natural water.

As proven earlier,<sup>27,28,50</sup> SBA-15 required only a very short time for the adsorption of pollutants from water (Figure S7). All experiments on sorption were carried out overnight. The kinetic curve for SBA-DA could be described by a pseudo-second-order equation, which indicated the inclusion of different types of ammonium groups in the complex. A comparison of the content of amino groups with the amount of adsorbate indicated the possible interaction of 1 PFOA molecule with 3 (in the case of SBA-NH), or the formation of 1:1 complexes in the case of other amino-containing materials; i.e., a higher concentration of ammonium groups contributed to the simplification of the complex to  $\sim 1/1$  (Table S1). By analyzing the features of PFOA sorption, namely, the correlation coefficients of the isotherm data with the equations of the Langmuir and Freundlich isotherms (Table 5), it can be concluded that the adsorption by SBA-NH and SBA-TA samples indicated an inhomogeneity of their surface. At the same time, only the Langmuir isotherm was suitable for the SBA-DA sample, indicating a mostly homogeneous surface layer and the predominant ion-exchange

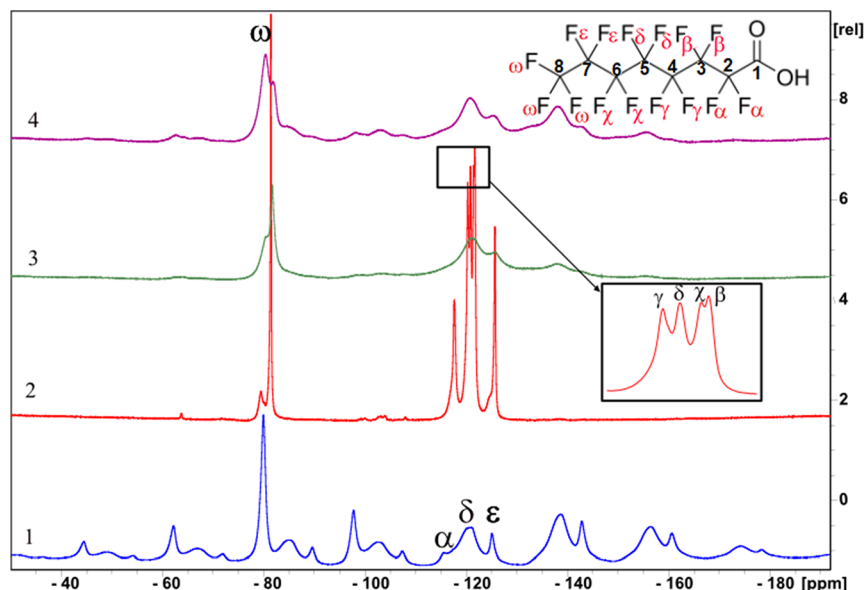


Figure 7. Solid-state  $^{19}\text{F}$  NMR spectra of the initial crystalline PFOA (1), SBA (2), SBA-DA (3), and SBA-TA (4).

Table 3. Chemical Shift Data for Uncomplexed and Complexed PFOA at Different Adsorbents with Chemical Shifts for Broad  $\text{CF}_3$  Components

position of the F atom	uncomplexed PFOA	SBA	SBA-DA	SBA-TA
$\omega$	-80.1	79.6, -81.2	-80.4, -82.0	-80.4, -81.9,
$\alpha$	-115.4	-117.5		
$\gamma$		-120.3		
$\delta$	-120.9	-120.7		-120.8
$\chi$		-121.5	-121.1	
$\beta$		-121.7		
$\epsilon$	-125.3	-125.7	-125.7	-125.4

Table 4. Content of F after Sorption from EDX<sup>a</sup>

sample	$\omega_{\text{F}}$ , % in the sorbent	ratio Si:F sample	$\omega_{\text{F}}$ , % in the solution
SBA	1.1	7.9:1	0.5
SBA-NH	12.6	1:1.0	0
SBA-DA	32.8	1:4.4	0
SBA-TA	28.1	1:4.7	0

<sup>a</sup>Notes:  $m = 0.02$  g,  $V_{\text{sol}} = 5$  mL,  $c = 0.012$  mol/L.

mechanism of adsorption. The “bare” SBA isotherm curve indicated that with low concentrations of PFOA in solution, sorption of molecules by silica did not occur due to the absence of chemical adsorption centers, while in more concentrated solutions of PFOA, physical sorption of

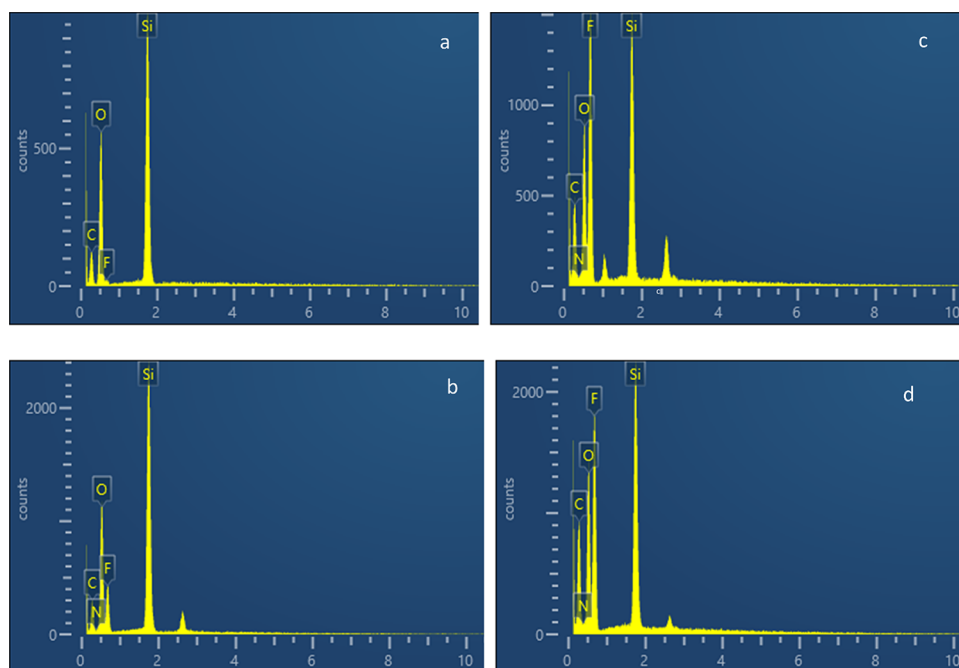
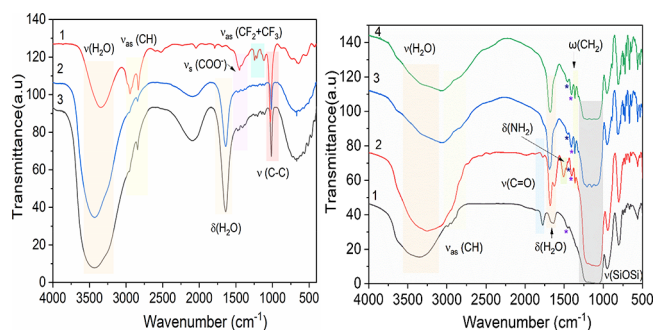


Figure 8. EDX of the SBA samples after adsorption for (a) SBA, (b) SBA-NH, (c) SBA-DA, and (d) SBA-TA.



**Figure 9.** Infrared spectra of PFOA for (a) (1) 0.1 mol/L solution in methanol, (2) 0.012 mol/L in water after sorption by SBA, and (3) 0.012 mol/L in water; and (b) adsorbed on silica sorbents (1 = SBA, 2 = SBA-NH, 3 = SBA-DA, 4 = SBA-TA,  $C_{\text{PFOA}} = 0.012$  mol/L, time = 12 h,  $t = 25$  °C).

molecules occurred due to adhesion. However, as was previously shown by NMR, PFOA on the surface of the silica sample was present in an unbound form. All PFOAs was washed out of the samples with alcohol and water, which may indicate ion-exchange and electrostatic adsorption mechanisms as well as the possibility of sorbent regeneration for further recovery.

These data and the acquired knowledge provide a background for the synthesis of newly tailored hybrid functionalized adsorbents. The sorbents of this class show promise at sites of significant accumulation of fluorine-containing pollutants, particularly in places of large-scale accidents and fires. There is also a possibility of using such adsorbents for fine cleaning as they can be used as fillers in

water treatment plants with a cumulative effect, an avenue that will be studied in future work.

## CONCLUSIONS

By combining the morphology of the sorbent, ensuring accessibility of all sorption centers, with chemical functionality, in our case, amine-containing groups, it was possible to increase the efficiency of PFOA removal due to the synergistic interplay of surface morphology and functionality. In addition, the strengthening of the electrostatic interaction of PFAS molecules with the functional groups of the adsorbent and the facility of hydrophobic interaction between the sorbent and PFAS molecules contributed significantly to the sorption capacity. Optimization of the synthesis will ensure the simplicity and cost-efficiency of the process in comparison with traditional sorbents.

As a result of the study, a number of highly efficient polyfunctional organo-inorganic hybrid materials were synthesized as sorbents of PFAS. The materials synthesized according to our developed techniques displayed high functional group content and had a specific surface area and structure, a narrow pore size distribution, and magnetic properties. The materials were hydrolytically stable at a wide pH range and could be regenerated, permitting repetitive and cyclic use for the complete removal of contaminants. Amino groups were protonated, contributing to a better interaction with PFOA, and could be grafted in different amounts on the surface of the sorbent.

The sorption capacity of inorganic porous materials toward PFOA was influenced by both the nature of the surface functional groups of the sorbents and the molecular structure of PFOA itself (e.g., size, hydrophobicity/hydrophilicity, and

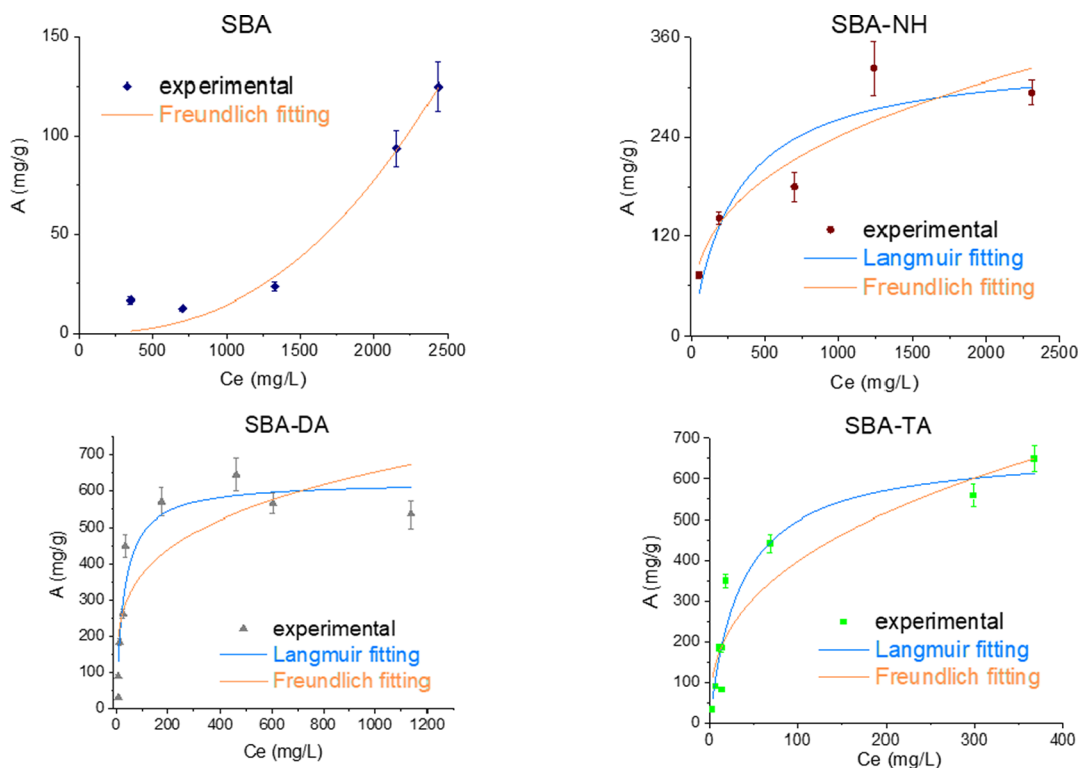


**Figure 10.** Adsorption isotherms of PFOA on SBA, SBA-NH, SBA-DA, and SBA-TA samples (conditions: pH = 2.34–3.34, adsorbent dose: 0.02 g, volume: 5 mL).

Table 5. Parameters of PFOA Adsorption by the Synthesized Samples<sup>a</sup>

PFOA Kinetic Sorption Parameters for SBA-DA									
adsorbate	pseudo (I) order $A_t = A_{eq} \times (1 - e^{-k_1 t})$				pseudo (II) order $A_t = \frac{k_2 A_{eq}^2 t}{1 + k_2 A_{eq} t}$				
	$A_{eq}$ , mg/g	$k_1$ , min <sup>-1</sup>	SD, mg/g	$R_{adj}^2$	$A_{eq}$ , mg/g	$k_2$ , L/mg min	SD, mg/g	$R_{adj}^2$	
PFOA	550 ± 10	0.09 ± 0.01	19	0.905	570 ± 30	$4 \times 10^{-4} \pm 1 \times 10^{-4}$	31	0.752	
PFOA Adsorption Parameters Estimated by Langmuir and Freundlich Isotherm Models									
sample	sorption capacity, mg/g	Langmuir equation				Freundlich equation			
		$A_{eq} = A_{max} \times K_L \times c_e / (1 + K_L \times c_e)$	$A_{max}$ , mg/g	$K_L$ , L/mg	SD, mg/g	$R_{adj}^2$	$A_{eq} = K_F \times c_e^{1/n}$	$K_F$ , L <sup>1/n</sup> mg <sup>1-1/n</sup> /g	$n$
SBA	125.0					$7 \times 10^{-7} \pm 2 \times 10^{-6}$	2.4 ± 0.5	10	0.962
SBA-NH	294.3	340 ± 60	0.003 ± 0.001	46	0.804	22 ± 9	0.35 ± 0.09	45	0.816
SBA-DA	569.5	620 ± 40	0.033 ± 0.008	73	<b>0.901</b>	120 ± 50	0.24 ± 0.07	131	0.678
SBA-TA	649.1	670 ± 60	0.028 ± 0.007	66	<b>0.913</b>	70 ± 20	0.38 ± 0.06	85	0.854

<sup>a</sup>Notes: highest values of correlation coefficients of  $R_{adj}^2$  and lowest values of SD are highlighted in bold.

polarity). Protonated amino groups can interact with PFOA due to electrostatic attraction, hydrogen bonding, and the van der Waals interaction. The observed interaction mechanism is rather general and should be useful for the removal of PFAA with both shorter and longer chain lengths. Based on the adsorption mechanism as understood in this work, there is a reasonable potential for regenerability.

## ■ ASSOCIATED CONTENT

### SI Supporting Information

The Supporting Information is available free of charge at <https://pubs.acs.org/doi/10.1021/acsestwater.3c00408>.

Experimental data, including EDX for all samples; DTG and TG analysis of N-containing SBA; NMR spectra of initial solution 0.001 mol/L of PFOA and solution of this concentration after sorption by SBA-DA; NMR spectra of initial solution 0.012 mol/L of PFOA and solution of this concentration after sorption by SBA-DA; dependence of the intensities of the <sup>19</sup>F resonances belonging to the compounds left in solution (H<sub>2</sub>O) after absorption on the synthesized samples (PDF)

## ■ AUTHOR INFORMATION

### Corresponding Authors

**Oksana Dudarko** – Department of Molecular Sciences, Swedish University of Agricultural Sciences, Uppsala SE-75007, Sweden; Chuiko Institute of Surface Chemistry of NAS of Ukraine, Kyiv 03164, Ukraine; [orcid.org/0000-0002-8353-8089](https://orcid.org/0000-0002-8353-8089); Email: [oksana.dudarko@slu.se](mailto:oksana.dudarko@slu.se)

**Gulaim Seisenbaeva** – Department of Molecular Sciences, Swedish University of Agricultural Sciences, Uppsala SE-75007, Sweden; [orcid.org/0000-0003-0072-6082](https://orcid.org/0000-0003-0072-6082); Email: [gulaim.seisenbaeva@slu.se](mailto:gulaim.seisenbaeva@slu.se)

### Authors

**Tetyana Budnyak** – Department of Materials Science and Engineering, Nanotechnology and Functional Materials, Uppsala University, Uppsala SE-751 03, Sweden; [orcid.org/0000-0003-2112-9308](https://orcid.org/0000-0003-2112-9308)

**Oleg Tkachenko** – Department of Materials Science and Engineering, Nanotechnology and Functional Materials, Uppsala University, Uppsala SE-751 03, Sweden; [orcid.org/0000-0002-2765-8625](https://orcid.org/0000-0002-2765-8625)

**Tatiana Agback** – Department of Molecular Sciences, Swedish University of Agricultural Sciences, Uppsala SE-75007, Sweden

**Peter Agback** – Department of Molecular Sciences, Swedish University of Agricultural Sciences, Uppsala SE-75007, Sweden

**Björn Bonnet** – Department of Aquatic Science and Assessment, Swedish University of Agricultural Sciences, Uppsala SE-750 07, Sweden

**Lutz Ahrens** – Department of Aquatic Science and Assessment, Swedish University of Agricultural Sciences, Uppsala SE-750 07, Sweden; [orcid.org/0000-0002-5430-6764](https://orcid.org/0000-0002-5430-6764)

**Geoffrey Daniel** – Department of Forest Biomaterials and Technology, Swedish University of Agricultural Sciences, Uppsala SE-750 07, Sweden

Complete contact information is available at:

<https://pubs.acs.org/10.1021/acsestwater.3c00408>

### Author Contributions

O.D.: conceptualization, investigation; methodology; writing-original draft preparation; O.T.: investigation of N<sub>2</sub> adsorption, fitting of kinetic and equilibrium isotherms; T.B.: formal analysis, T.A.: interpretation of NMR results, P.A.: investigation of the samples by of NMR, B.B.: investigation of adsorption PFOA, L.A.: interpretation of adsorption PFOA, writing of manuscript, G.D.: investigation of the samples by TEM, G.A.S.: conceptualization, validation, editing, project supervision, funding acquisition.

### Funding

VR-2018-04841 “Multifunctional hybrid adsorbents for water purification”, Wenner-Gren Foundation GFU 2022-0024.

### Notes

The authors declare no competing financial interest.

## ■ ACKNOWLEDGMENTS

The corresponding authors are grateful for financial support from the Wenner-Gren Foundation.

## ■ REFERENCES

(1) Koban, L. A.; Pfluger, A. R. Per- and polyfluoroalkyl substances (PFAS) exposure through munitions in the Russia-Ukraine conflict. *Integr. Environ. Assess. Manag.* **2023**, *19*, 376–381.

- (2) Post, G. B.; Cohn, P. D.; Cooper, K. R. Perfluorooctanoic acid (PFOA), an emerging drinking water contaminant: a critical review of recent literature. *Environ. Res.* **2012**, *116*, 93–117.
- (3) Meegoda, J. N.; Bezerra de Souza, B.; Monteiro Casarini, M.; Kewalramani, J. A. A Review of PFAS Destruction Technologies. *Int. J. Environ. Res. Public Health* **2022**, *19*, 16397.
- (4) Ahrens, L.; Bundschuh, M. Fate and effects of poly- and perfluoroalkyl substances in the aquatic environment: A review. *Environ. Toxicol. Chem.* **2014**, *33*, 1921–1929.
- (5) An official site of Société Générale de Surveillance SA Physical and chemical properties of PFAS compounds Physical-and-Chemical-Properties-of-PFAS-compounds\_vKFMH.pdf (sgs-ehsusa.com).
- (6) Fagbayigbo, B. O.; Opeolu, O. S.; Fatoki, O. S.; Olatunji, M. O.; Akharam, M. O.; Human, I. S. Sorption and partitioning of perfluorooctanoic acid (PFOA) and perfluorooctane sulfonate (PFOS) onto sediments of Diep and Plankenburg river systems Western Cape, South Africa. *Hum. Environ. Technol. Innov.* **2022**, *25*, No. 102110.
- (7) An official website of the European Union. *Directive (EU) 2020/2184 of the European Parliament and of the Council of 16 December 2020 on the quality of water intended for human consumption (recast) (Text with EEA relevance)*; <https://eur-lex.europa.eu/eli/dir/2020/2184/oj> (accessed February 2022).
- (8) An official website of Danish Hydraulic Institute. *Sweden tightens up on substance requirements for drinking water*; [tox.dhi.dk/en/news/news/article/sweden-tightens-up-on-substance-requirements-for-drinking-water/#:~:text=In a new bill the Swedish Food Agency, with the values for arsenic%2C lead and cadmium](https://tox.dhi.dk/en/news/news/article/sweden-tightens-up-on-substance-requirements-for-drinking-water/#:~:text=In a new bill the Swedish Food Agency, with the values for arsenic%2C lead and cadmium) (accessed February 2022).
- (9) An official page Swedish Food Agency. *The Swedish Food Agency's regulations on drinking water LIVSFS 2022:12 (livsmedelsverket.se)*; (accessed November 2022).
- (10) Appleman, T. D.; Dickenson, E. R. V.; Bellona, C.; Higgins, C. P. Nanofiltration and granular activated carbon treatment of perfluoroalkyl acids. *J. Hazard* **2013**, *260*, 740.
- (11) Im, S.-J.; Lee, H.; Jang, A. Effects of co-existence of organic matter and microplastics on the rejection of PFCs by forward osmosis membrane. *Environ. Res.* **2021**, *194*, No. 110597.
- (12) Li, M.; Sun, F.; Shang, W.; Zhang, X.; Dong, W.; Dong, Z.; Zhao, S. Removal mechanisms of perfluorinated compounds (PFCs) by nanofiltration: Roles of membrane-contaminant interactions. *Chem. Eng. J.* **2021**, *406*, No. 126814.
- (13) Hang, X.; Chen, X.; Luo, J.; Cao, W.; Wan, Y. Removal and recovery of perfluorooctanoate from wastewater by nanofiltration. *Sep. Purif. Technol.* **2015**, *145*, 120.
- (14) Kazwini, T.; Yadav, S.; Ibrar, I.; Al-Juboori, R. A.; Singh, L.; Ganbat, N.; Karbassiyazdi, E.; Samal, A. K.; Subbiah, S.; Altaee, A. Updated review on emerging technologies for PFAS contaminated water treatment. *Chem. Eng. Res. Des.* **2022**, *182*, 667.
- (15) Militao, I. M.; Roddick, F. A.; Bergamasco, R.; Fan, L. Removing PFAS from aquatic systems using natural and renewable material-based adsorbents: A review. *J. of Environ.* **2021**, *9*, No. 105271.
- (16) Duan, C.; Shen, Z.; Wu, D.; Guan, Y. Recent developments in solid-phase microextraction for on-site sampling and sample preparation. *TrAC. Trends Anal. Chem.* **2011**, *30*, 1568.
- (17) Otlés, S.; Ozyurt, V. H. Sampling and sample preparation. In *Handbook of Food Chemistry*; Cheung, P., Ed.; Springer: Berlin, Heidelberg, 2015.
- (18) Kucharzyk, K. H.; Darlington, R.; Benotti, M.; Deeb, R.; Hawley, E. Novel treatment technologies for PFAS compounds: A critical review. *J. Environ. Manag* **2017**, *204*, 757.
- (19) Ross, L.; McDonough, J.; Miles, J.; Storch, P.; Kochunaryanan, P. T.; Kalve, E.; Hurst, J.; Dasgupta, S. S.; Burdick, J. A Review of Emerging Technologies for Remediation of PFASs. *Remediation* **2018**, *28*, 101–126.
- (20) Ateia, M.; Alsbaiee, A.; Karanfil, T.; Dichtel, W. Efficient PFAS Removal by Amine-Functionalized Sorbents: Critical Review of the Current Literature. *Environ. Sci. Technol. Lett.* **2019**, *6*, 688.
- (21) Du, Z.; Deng, S.; Bei, Y.; Huang, Q.; Wang, B.; Huang, J.; Yu, G. Adsorption behavior and mechanism of perfluorinated compounds on various adsorbents review. *J. Hazard.* **2014**, *274*, 443.
- (22) Pourreza, N.; Rastegarzadeh, S.; Larki, A. Simultaneous preconcentration of Cd(II), Cu(II) and Pb(II) on Nano-TiO<sub>2</sub> modified with 2-mercaptobenzothiazole prior to flame atomic absorption spectrometric determination. *J. Ind. Eng. Chem.* **2014**, *20*, 2680.
- (23) Jakavula, S.; Biata, N. R.; Dimpe, K. M.; Pakade, V. E.; Nomngongo, P. N. A critical review on the synthesis and application of ion-imprinted polymers for selective preconcentration, speciation, removal and determination of trace and essential metals from different matrices. *Crit. Rev. Anal. Chem.* **2022**, *52* (2), 314.
- (24) Sliesarenko, V. V.; Dudarko, O. A.; Zub, Y. L.; Seisenbaeva, G. A.; Kessler, V. G.; Topka, P.; Solcová, O. One-pot synthesis of mesoporous SBA-15 containing protonated 3-aminopropyl groups. *J. of Porous Mater.* **2013**, *20* (5), 1315.
- (25) Sliesarenko, V. V.; Dudarko, O. A.; Shcherbatyuk, N. N.; Zub, Y. L. Production of SBA-15 mesoporous silica containing ammonium groups in the surface layer. *Prot. Met. Phys. Chem. Surf.* **2014**, *50* (3), 293–299.
- (26) Stolyarchuk, N. V.; Tomina, V. V.; Mishra, B.; Tripathi, B. P.; Vaclavikova, M.; Dudarko, O. A.; Melnyk, I. V. Direct synthesis of efficient silica-based adsorbents carrying EDTA groups for the separation of Cu(II) and Ni(II) ions. *Colloids Surf. A Physicochem. Eng. Asp.* **2022**, *650*, No. 129538.
- (27) Kobylinska, N. G.; Kessler, V. G.; Seisenbaeva, G. A.; Dudarko, O. A. In situ Functionalized Mesoporous Silicas for Sustainable Remediation Strategies in Removal of Inorganic Pollutants from Contaminated Environmental Water. *ACS Omega* **2022**, *7* (27), 23576.
- (28) Kobylinska, N.; Dudarko, O.; Kessler, V.; Seisenbaeva, G. Enhanced Removal of Cr(III), Mn(II), Cd(II), Pb(II) and Cu(II) from Aqueous Solution by N-functionalized Ordered Silica. *Chemistry Africa* **2021**, *4* (2), 451.
- (29) Dudarko, O.; Zub, Y. Synthesis of SBA-15 type organosilica sorbents using sodium metasilicate and phosphonic acid residues. *Chem. J. Mold.* **2017**, *12* (2), 79.
- (30) Dudarko, O. A.; Barany, S. Synthesis and characterization of sulfur-containing hybrid materials based on sodium silicate. *RSC Adv.* **2018**, *8* (65), 37441.
- (31) Smith, S. J.; Wiberg, K.; McCleaf, P.; Ahrens, L. Pilot-Scale Continuous Foam Fractionation for the Removal of Per- And Polyfluoroalkyl Substances (PFAS) from Landfill Leachate. *ACS. Environ. Sci. Technol. W.* **2022**, *2*, 841.
- (32) Ho, Y.-S. Review of second-order models for adsorption systems. *Journal of Hazardous Materials* **2006**, *136* (3), 681.
- (33) Dudarko, O.; Kobylinska, N.; Kessler, V.; Seisenbaeva, G. Recovery of rare earth elements from NdFeB magnet by mono- and bifunctional mesoporous silica: Waste recycling strategies and perspectives. *Hydrometallurgy* **2022**, *210*, No. 105855.
- (34) Dudarko, O. A.; Gunathilake, C.; Sliesarenko, V. V.; Zub, Y. L.; Jaroniec, M. Microwave-assisted and conventional hydrothermal synthesis of ordered mesoporous silicas with P-containing functionalities. *Colloids Surf. A Physicochem. Eng. Asp.* **2014**, *459*, 4.
- (35) Jaroniec, M.; Solovyov, L. A. Assessment of ordered and complementary pore volumes in polymer templated mesoporous silicas and organosilicas. *Chem. Commun.* **2006**, 2242–2244, DOI: 10.1039/B604283J.
- (36) Rouquerol, F.; Rouquerol, J.; Sing, K. S. W. *Adsorption by powders and porous solids. Principles, methodology and applications*; Academic Press: New York, 1999.
- (37) Horikawa, T.; Do, D. D.; Nicholson, D. Capillary condensation of adsorbates in porous materials. *Adv. Colloid Interface Sci.* **2011**, *169* (1), 40.
- (38) Deng, S.; Niu, L.; Bei, Y.; Wang, B.; Huang, J.; Yu, G. Adsorption of perfluorinated compounds on aminated rice husk prepared by atom transfer radical polymerization. *Chemosphere* **2013**, *91* (2), 124.

- (39) Du, Z.; Deng, S.; Bei, Y.; Huang, Q.; Wang, B.; Huang, J.; Yu, G. Adsorption behavior and mechanism of perfluorinated compounds on various adsorbents—A review. *J. Hazard.* **2014**, *274*, 443–454.
- (40) Wang, X.; Long, P.; Dong, S.; Hao, J. First fluorinated zwitterionic micelle with unusually slow exchange in an ionic liquid. *Langmuir* **2013**, *29*, 14380.
- (41) Söderman, O.; Stilbs, P.; Price, W. S. NMR studies of surfactants. *Concepts in Magnetic Resonance Part A* **2004**, *23A* (2), 121.
- (42) Ning, C.; Ma, H.; Pedersen, C. M.; Chang, H.; Wang, Y.; Qiao, Y. Interaction between environmental contaminant PFOA and PAMAM in water: <sup>19</sup>F and <sup>1</sup>H NMR studies. *J. Mol. Liq.* **2019**, *283*, 45.
- (43) Dong, S. L.; Xu, G. Y.; Hoffmann, H. Aggregation behavior of fluorocarbon and hydrocarbon cationic surfactant mixtures: a study of (<sup>1</sup>H NMR and (<sup>19</sup>F NMR. *J. Phys. Chem. B* **2008**, *112*, 9371.
- (44) Blesic, M.; Marques, M. H.; Plechkova, N. V.; Seddon, K. R.; Rebelo, L. P. N.; Lopes, A. Self-aggregation of ionic liquids: micelle formation in aqueous solution. *Green Chem.* **2007**, *9*, 481.
- (45) Karoyo, A. H.; Borisov, A. S.; Wilson, L. D.; Hazendonk, P. Formation of Host-Guest Complexes of  $\beta$ -Cyclodextrin and Perfluorooctanoic Acid. *J. Phys. Chem. B* **2011**, *115*, 9511.
- (46) Gao, X.; Chorover, J. Adsorption of perfluorooctanoic acid and perfluorooctanesulfonic acid to iron oxide surfaces as studied by flow-through ATR-FTIR spectroscopy. *Environ. Chem.* **2012**, *9* (2), 148.
- (47) Zhang, Z.; Sarkar, D.; Datta, R.; Deng, Y. Adsorption of perfluorooctanoic acid (PFOA) and perfluorooctanesulfonic acid (PFOS) by aluminum-based drinking water treatment residuals. *J. Hazard. Mater.* **2021**, *2*, No. 100034.
- (48) Yu, Q.; Zhang, R.; Deng, S.; Huang, J.; Yu, G. Sorption of perfluorooctane sulfonate and perfluorooctanoate on activated carbons and resin: kinetic and isotherm study. *Water Res.* **2009**, *43* (4), 1150.
- (49) Wang, F.; Shih, K. Adsorption of perfluorooctanesulfonate (PFOS) and perfluorooctanoate (PFOA) on alumina: influence of solution pH and cations. *Water Res.* **2011**, *45* (9), 2925.
- (50) Fetisova, Y. S.; Dudarko, O. A.; Bauman, M.; Lobnik, A.; Sliesarenko, V. V. Adsorption of lead(II), cadmium(II) and dysprosium(III) from aqueous solutions using mesoporous silica modified with phosphonic acid groups. *J. Solgel. Sci. Technol.* **2018**, *88* (1), 66.